


Constriction of Actin Rings by Passive Crosslinkers

Alexander Cumberworth^{✉*} and Pieter Rein ten Wolde[†]
 AMOLF, Science Park 104, 1098 XG Amsterdam, Netherlands

 (Received 4 March 2022; accepted 6 June 2023; published 17 July 2023)

In many organisms, cell division is driven by the constriction of a cytokinetic ring, which consists of actin filaments and crosslinking proteins. While it has long been believed that the constriction is driven by motor proteins, it has recently been discovered that passive crosslinkers that do not turn over fuel are able to generate enough force to constrict actin filament rings. To study the ring constriction dynamics, we develop a model that includes the driving force of crosslinker condensation and the opposing forces of friction and filament bending. We analyze the constriction force as a function of ring topology and crosslinker concentration, and predict forces that are sufficient to constrict an unadorned plasma membrane. Our model also predicts that actin-filament sliding arises from an interplay between filament rotation and crosslinker hopping, producing frictional forces that are low compared with those of crosslinker-mediated microtubule sliding.

DOI: [10.1103/PhysRevLett.131.038401](https://doi.org/10.1103/PhysRevLett.131.038401)

In animals, fungi, and some closely related unicellular eukaryotes, cytokinesis is driven by the assembly and constriction of a ring composed of actin filaments and a number of actin-binding proteins [1–3]. It is widely believed that the constriction forces in the ring are generated by myosin, a motor protein that drives the sliding of actin filaments along each other in an active process using fuel turnover [4–10]. However, ring constriction and successful cell division have been observed with impaired myosin motor activity [11], particularly in budding yeast [12–14]. Furthermore, it was recently found that passive crosslinking proteins, which do not turn over fuel, are also able to produce sliding forces, either via the entropy associated with the diffusion of the crosslinkers within the overlap region between the filaments, or via their condensation from the solution to the overlap region [15]. Even more recently, it has been shown that passive actin crosslinkers can not only induce the assembly of actin filaments into rings, but also even drive the constriction of these rings [16]. Yet, it remains unclear what the magnitude of the constriction force is that can be generated via this mechanism, how this force depends on the concentration of the crosslinkers and the stiffness and configuration of the filaments, and whether these forces would be sufficient to drive cell constriction. Finally, given that microtubule sliding driven by passive crosslinkers rapidly stalls because the friction becomes prohibitive [15,17], it is also unclear how actin rings are able to constrict on experimental timescales [16].

Here, we develop an analytical model that accounts for the sliding force from passive filament crosslinkers and the opposing forces stemming from the bending of filaments and the friction of sliding. The details of our model are based on the anillin-actin system of Ref. [16], although we emphasize that the framework of the model is more generic,

applying to any system consisting of filaments that are crosslinked by proteins that passively bind to discrete binding sites. We show under what conditions a ring at equilibrium is possible, and how the force depends on the ring radius for different filament lengths, topologies, and crosslinker concentrations. The force generated by such a ring would be sufficient to constrict an unadorned plasma membrane, and could be of interest for building the division machinery in a minimal synthetic cell. Lastly, our model predicts that the frictional force scales exponentially with the number of bound crosslinkers, in contrast with the super-exponential scaling of crosslinker-mediated microtubule sliding [17], allowing for ring constriction on minute time-scales [16].

In order to model the contractile rings, we need an expression for the energy of filament sliding when passive crosslinkers are present. In this case, the sliding force is a condensation force, i.e., the sliding is driven by the binding of more crosslinkers as the overlap increases [15]. Both Lansky *et al.* [15] and Wierenga [18] derived analytical expressions for a condensation force where the binding and unbinding of the crosslinkers were assumed to be fast relative to filament sliding. Here, as in Ref. [18], we assume that the crosslinkers can either bind once to a single filament or to a pair of binding sites, such that they bundle two filaments (see the Supplemental Material [19] for discussion of anillin-actin bundling). If the binding sites are separated by a distance of δ_d , then the overlap length is $L = \delta_d(l - 1)$, where l is the number of binding site pairs [Fig. 1(a)]. The free energy is then given by [18]

$$\Delta\Phi_S = -\frac{k_B T L}{\delta_d} \ln(1 + \xi), \quad \xi = \frac{K_D^s [X]}{K_D^d (K_D^s + [X])^2}, \quad (1)$$

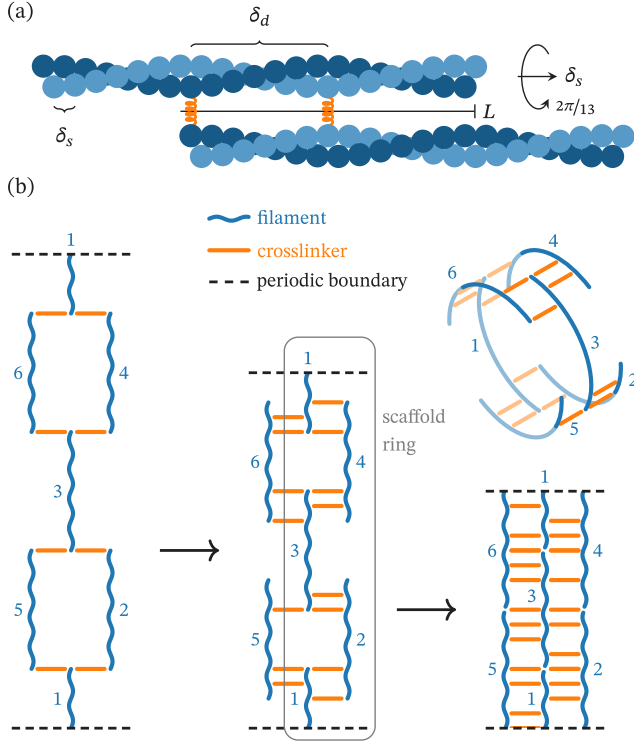


FIG. 1. (a) Diagram of a single overlap of length L formed by two actin filaments. The half helical pitch determines the distance between crosslinking sites δ_d rather than the monomer-monomer distance δ_s . Filaments slide in increments of δ_s , which requires a rotation of $2\pi/13$. (b) Diagrams of a ring constricting to half its radius. The 2D diagrams use periodic boundary conditions. On the left, the ring is at its maximum radius R_{\max} ; in the middle, it has constricted to three quarters of R_{\max} ; on the right, it has reached its minimum radius $R_{\min} = R_{\max}/2$. In the top right, a 3D representation of the topology diagram in the center is given. In this example, the number of filaments in the scaffold ring N_{sca} is 4, while the total number of filaments N_f is 6. Note that while N_{sca} is unique, the scaffold ring is not; here, it could instead be defined by filaments 1, 3, 5, and 6.

where T is the temperature, $[X]$ is the concentration of anillin, K_D^s is the dissociation constant of anillin binding to a single actin filament, K_D^d is the dissociation constant of anillin crosslinking two actin filaments from solution, and k_B is the Boltzmann constant. The linear dependence of $\Delta\Phi_S$ on L means that the sliding force, given by the derivative of Eq. (1), does not depend on the overlap length.

Because the sliding force is independent of the overlap length, the ring-constriction force depends only on the total number of overlaps, and hence the connectivity of the filaments, or in other words, the topology of the ring. We consider stable rings wherein all filaments are under tension and hence contribute to the constriction force (i.e., those filaments that have overlaps on either end; see the Supplemental Material [19] for further discussion). To characterize the ring topology, we introduce the notion of a ‘‘scaffold ring’’ [Figs. 1(b), 2(a), and S1(a) in

the Supplemental Material [19]]. The scaffold ring is defined by the smallest set of filaments that still form a ring, and N_{sca} is defined to be the number of filaments in that ring. Making the simplifying assumption that all filaments have the same length, the number of overlaps in the ring is determined by N_{sca} and the total number of filaments in the ring N_f [Fig. 1(b)]. In a scaffold ring, each filament forms two overlaps, making the number of overlaps equal to the number of filaments. However, each additional filament will add two more overlaps to the ring; the total number of overlaps is thus $N_o = 2N_f - N_{\text{sca}}$.

To derive the total free energy of the ring as a function of the radius, we need an expression for the total overlap length L_{tot} as a function of the radius R . If we make the further simplifying assumption that all filaments overlap to the same degree, then N_{sca} also determines this relationship: the length of each overlap L is the difference between the filament length L_f and the current ring circumference divided by N_{sca} . Then, the total overlap length is

$$L_{\text{tot}} = N_o L = (2N_f - N_{\text{sca}}) \left(L_f - \frac{2\pi R}{N_{\text{sca}}} \right). \quad (2)$$

This expression reveals that the maximum radius R_{\max} , where $L_{\text{tot}} = 0$, is $R_{\max} = N_{\text{sca}} L_f / 2\pi$. We restrict the minimum radius R_{\min} to be $R_{\max}/2$ because of an energy barrier due to steric clashing that begins to occur at this point as the filaments run into each other; see also the Supplemental Material [19].

The final element in deriving an expression for the constriction force is an expression for the energy required to bend the filaments into a ring. If we treat the ring as a simple linearly elastic rod, and assume that the ring geometry is perfectly circular (the full derivation and justifications for these assumptions are given in the Supplemental Material [19]), then the bending energy is

$$U_B = \frac{N_f E I L_f}{2R^2}, \quad (3)$$

where E is the Young’s modulus, I is the second moment of area, and R is the ring radius. Then, multiplying Eq. (1) by N_o and combining it with Eqs. (2) and (3) allows us to write the total free energy, the derivative of which gives the radial constriction force,

$$F = -\frac{2\pi k_B T (2N_f - N_{\text{sca}})}{N_{\text{sca}} \delta_d} \ln(1 + \xi) + \frac{N_f E I L_f}{R^3}. \quad (4)$$

In equilibrium, the sliding force is balanced by the opposing bending force such that the net force F is zero; solving Eq. (4) for $F = 0$ then yields the equilibrium radius R_{eq} .

With Eq. (4), we can calculate the free energies and constriction forces as a function of the radius, as well as the equilibrium radius for a given set of parameters. In the

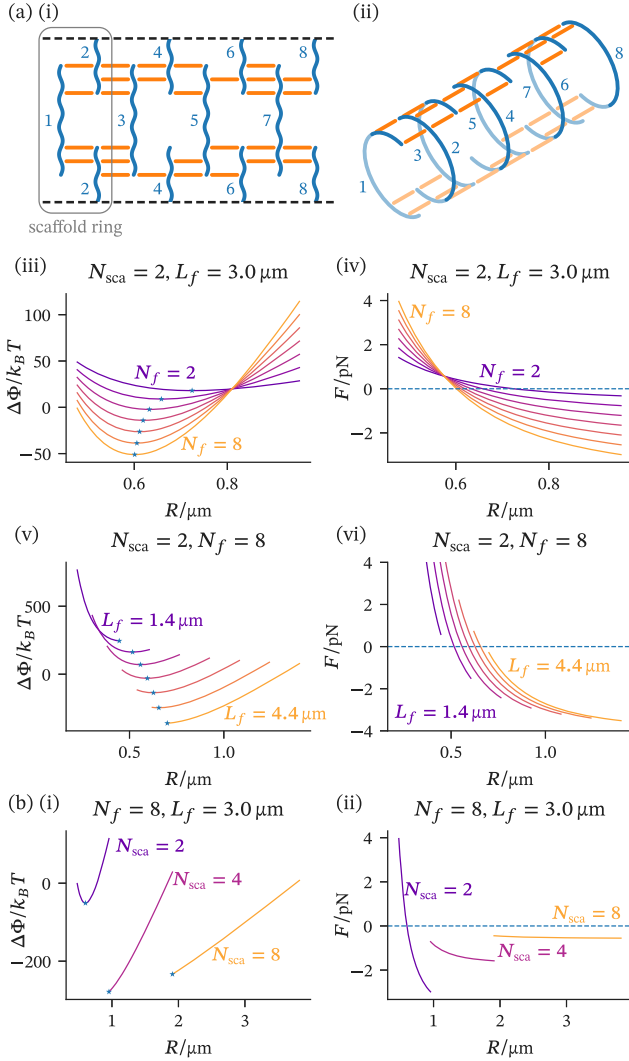


FIG. 2. Total free energy $\Delta\Phi$ and total force F as a function of the ring radius. The blue stars indicate the points at which the free energy is minimal, and negative force values indicate a constricting force. In (a), $N_{\text{sca}} = 2$, as per the topology depicted with both 2D periodic boundary conditions (i) and in 3D (ii); the free energies and total forces are then plotted for either a range of N_f values [(iii) and (iv)] or a range of L_f values [(v) and (vi)]. The constriction force increases linearly with N_f . In (b), $N_f = 8$, and the free energies (i) and total forces (ii) are plotted for three values of N_{sca} (see Fig. S1 in the Supplemental Material [19] for associated topology diagrams). Connecting the filaments in series (large N_{sca}) increases the constriction range, while stacking them in parallel (small N_{sca}) increases the maximum constriction force. Data for all plots were produced with the parameters given in Table S1 of the Supplemental Material [19].

study that observed the constricting rings [16], it was found that the rings have up to eight filaments, so we focus on this range of filaments here (see the Supplemental Material [19] for discussion of model parameters). At large radii, the sliding force dominates over the bending force, and the net force is negative (inward) (Fig. 2). The free energy and the

magnitude of the force then decrease as the radius decreases. For radii smaller than R_{eq} , the free energy increases and the net force becomes positive (outward), since the bending force becomes larger than the sliding force. As N_f increases for a given N_{sca} , R_{eq} first decreases, but then plateaus [Fig. 2(a)(iii)]. From Fig. 2(a)(iv) and Eq. (4), however, the initial constriction force can be seen to increase linearly with N_f for a given radius. Finally, for a given N_f , there is a trade-off between the range of radii over which the ring can generate force and the maximum possible force it can achieve. While connecting the filaments in series (large N_{sca}) favors the former, stacking them in parallel (small N_{sca}) favors the latter [Fig. 2(b)].

As can be seen from Eq. (4), there is an optimal anillin concentration that maximizes the force, specifically when $[X] = K_D^s$, after which point higher concentrations lead to lower sliding forces [18]. This decrease in the sliding force occurs because, at higher crosslinker concentrations, the entropy of mixing in solution favors the binding of crosslinkers to a single actin site instead of two, thus impeding crosslinking and hence the condensation force. In fact, the anillin concentration used in the experiments [16] happens to be close to K_D^s (Fig. S6 [19]).

Kučera *et al.* [16] observed that destabilized actin filaments can, paradoxically, lead to further constriction. Our model provides an explanation for this observation: as the filaments depolymerize and L_f decreases, the opposing bending force and hence R_{eq} decrease [Figs. 2(a)(v) and 2(a)(vi)].

So far, we have ignored the frictional forces involved in ring constriction. To study the timescale of ring constriction, we simulate the overdamped ring-constriction dynamics within our model. To do so, we require an expression for the friction coefficient of the ring.

Wierenga and Ten Wolde [17] derived the friction coefficient of the sliding of two crosslinked microtubules. The sliding mechanism involves a collective rearrangement of all the crosslinkers in the overlap, wherein the crosslinkers hop between neighboring sites on the microtubules. This collective rearrangement gives rise to an energy barrier that increases linearly with the number of bound crosslinkers N_d , and thus a friction coefficient that scales exponentially with N_d . Additionally, because the crosslinkers can block each other from hopping, the friction scales superexponentially with N_d at higher crosslinker densities.

In actin filaments, the distance between crosslinker binding sites δ_d is much larger than the distance over which crosslinkers can hop, as the distance between sites is set by the helical pitch rather than the monomer-monomer distance δ_s [44] [Fig. 1(a)]. This suggests that the above sliding mechanism may be unfeasible. However, actin filaments have been observed to twirl, or rotate, about their axes when they are being slid by myosin motor

proteins bound to a surface [45–50]. We postulate that passively crosslinked actin filaments must also twirl as they slide, which would allow crosslinkers to hop distances of δ_s (rather than the larger δ_d), thus also allowing the same collective rearrangement as was found for microtubules [Figs. 1(a) and S4 in the Supplemental Material [19]].

Because the crosslinkers are spaced at least δ_d apart, they do not block each other when hopping by δ_s to neighboring sites [Fig. 1(a)]. The friction coefficient therefore only scales exponentially with N_d , not superexponentially as with microtubule sliding [17]; as we will see, this difference has dramatic consequences. In the regime where crosslinker binding is fast relative to filament sliding and the average number of crosslinkers is a function of the overlap L , the friction coefficient of a single overlap is

$$\zeta = \zeta_0 \left[\frac{1 + \xi}{1 + \xi e^{-B}} \right]^{\left(\frac{L}{\delta_d} + 1\right)}. \quad (5)$$

Here, ξ is defined in Eq. (1) and

$$\zeta_0 = \frac{k_B T}{\delta_s^2 r_0} \sqrt{1 + \frac{3k\delta_s^2}{4k_B T}}, \quad B = \frac{\delta_s^2 k}{8k_B T} - \ln 2, \quad (6)$$

where k is the spring constant of the crosslinker, and r_0 is the jump-rate prefactor for crosslinker hopping (see the Supplemental Material [19] for full derivation). The friction coefficient of the ring ζ_R can be related to that of a single overlap ζ via $\zeta_R = 4\pi^2 N_o / N_{sca}^2 \zeta$ by considering the number of overlaps acting in series and in parallel (see the Supplemental Material [19] for full derivation).

Simulations with this expression for the friction coefficient show that the ring constriction occurs within experimental timescales [16] for the experimentally relevant range of model parameter values (Fig. 3). Of the

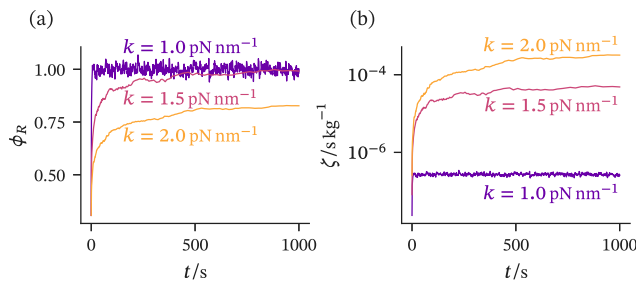


FIG. 3. Ring-constriction trajectories with $L_f = 3.0 \mu\text{m}$, $N_{sca} = 2$, $N_f = 5$, and three different values of k . (a) Progress of radial constriction from its maximum ($\phi_R = 0$) to its equilibrium value ($\phi_R = 1$), where $\phi_R = (R_{\text{max}} - R)/(R_{\text{max}} - R_{\text{eq}})$. (b) Friction coefficient of an overlap in the ring. For numerical details and additional quantities, see Fig. S8(a) in the Supplemental Material [19]; for trajectories with values of k down to 0.1 pN nm^{-1} , see Fig. S11 in the Supplemental Material [19]. For the biologically relevant range of k , constriction occurs on experimental timescales [16].

parameters, the spring constant has been shown to be the most critical [15,17]. While the value of k for anillin has not been measured, crosslinking proteins tend to be on the lower end of the range of values measured in proteins [17,51–61], with values falling within 0.3 and 1.2 pN nm^{-1} [17,54,59,61]. To explore the dynamics in this range of k , we first consider a ring with $N_{sca} = 2$, $N_f = 5$, and $L_f = 3.0 \mu\text{m}$, which leads to an equilibrium radius that is around halfway between the maximum and minimum possible radii [Fig. S7(b) in the Supplemental Material [19]]. With $k = 1.0 \text{ pN nm}^{-1}$, the ring constricts almost instantaneously (Fig. 3). Increasing the value to $k = 1.5 \text{ pN nm}^{-1}$ leads to much slower constriction, but the ring still reaches its equilibrium value within the timescale used in the experiments (1000 s) [16]. By $k = 2.0 \text{ pN nm}^{-1}$, the ring constriction stalls before reaching the equilibrium radius. Varying N_f [Figs. S8(b) and S9 in the Supplemental Material [19]] and using a different value of L_f (Fig. S10 in the Supplemental Material [19]) did not have a large impact on the dynamics. Overall, while microtubule sliding rapidly stalls because the friction becomes prohibitive [15], the much weaker scaling of the friction with N_d for anillin-actin rings means that the latter can constrict to their equilibrium radii on experimental timescales of minutes [16].

Even when the mean forces on either end of the filaments are balanced, thermal fluctuations will eventually break the ring. However, in Ref. [16], the rings were observed to be stable on the timescale of the experiments. During ring constriction, a mechanism exists that tends to equalize overlaps: if some overlaps fluctuate toward smaller values, then the ring-constriction force will tend to increase their overlap more quickly because they also then have a lower friction. Once the rings have reached equilibrium, we can estimate the timescale on which the ring is stable from $\tau = x^2/D_f$, where D_f is the diffusion coefficient of a single filament and x is the overlap length at equilibrium. The overlaps of a single filament act in parallel, so the total friction force experienced by a single filament is the sum of the friction of its n individual overlaps, which implies that the friction coefficient of a single filament is $\zeta_f = n\zeta$, and its associated diffusion coefficient is $D_f = k_B T/\zeta_f$. If we consider a filament with two overlaps, and use the overlap length of the rings modeled in Fig. 3 in equilibrium, $x = 0.75 \mu\text{m}$, as well as the value of the friction coefficient at equilibrium, $\zeta = 5 \times 10^{-4} \text{ s kg}^{-1}$, then $\tau = 14000 \text{ s}$. This is more than an order of magnitude longer than the experimental timescale. Further, this calculation assumes that the overlaps are equal in size, yet fluctuations away from this state will lengthen some overlaps at the expense of others, which tends to increase the friction the filament experiences. This estimate for τ thus gives a lower bound, strengthening the prediction that the rings are stable on much longer timescales than the experiments were performed on.

The tension T of cytokinetic rings, which is related to the constriction force F via $T = F/2\pi$, has been measured to be hundreds of pN in fission yeast [4,62], while here, using experimentally measured values of N_f , L_f , and R *in vivo* [63–65], the tension does not exceed 10 pN. However, even the measured ring tensions are nearly 3 orders of magnitude too small to balance measured turgor pressures and would, in fact, only produce strains in the cell wall of 0.01% [1]. Instead of directly constricting the cell, the cytokinetic ring in fission yeast coordinates and guides the inward growth of the cell wall via mechanosensitive enzymes [66,67]. For this function, even a much smaller ring tension may be sufficient, if less effective [67]. These findings in fission yeast, a model organism for eukaryotic division [68,69], are likely relevant more broadly in fungi; in budding yeast, a similar interplay between cell-wall growth and cytokinetic-ring constriction has been observed [70]. While the maximum tension generated by passive crosslinking is smaller than that generated by myosin motors in the cytokinetic ring, the mechanism may provide an explanation for the observations that budding yeast can divide without myosin motor activity [12–14], possibly in combination with other non-myosin-motor force generating mechanisms [71].

Regardless of the role of passive-crosslinker-driven constriction in natural cells, the anillin-actin system is an interesting candidate for a cell-division module in a minimal synthetic cell. Actin, under polymerizing conditions, can grow into rings centered at the equator of droplets with diameters less than the persistence length of actin [72]. Anillin, besides being a crosslinker of actin, also has domains which bind to lipid membranes, and it appears to play a key role in anchoring the cytokinetic ring to the membrane in animal cells [73]. Further, experiments [74] and modeling [75] indicate that constriction of unadorned lipid-membrane vesicles requires contractile forces on the order of a pN, well within the range that can be generated via this mechanism. Therefore, by coupling anillin expression to the cell cycle, the system studied here may constitute a minimal module for triggering cell division upon the completion of DNA replication [76].

The authors would like to thank Vahe Galstyan and Ramon Creyghton for their helpful comments on the manuscript. This work was supported by a Gravitation grant from the Netherlands Organization for Scientific Research (NWO) Gravitation, Building a Synthetic Cell (BaSyC) (024.003.019).

*alex@cumberworth.org

†tenwolde@amolf.nl

- [1] T. D. Pollard and B. O’Shaughnessy, Molecular mechanism of cytokinesis, *Annu. Rev. Biochem.* **88**, 661 (2019).
 [2] M. C. Mangione and K. L. Gould, Molecular form and function of the cytokinetic ring, *J. Cell Sci.* **132**, jcs.226928 (2019).

- [3] T. H. Cheffings, N. J. Burroughs, and M. K. Balasubramanian, Actomyosin ring formation and tension generation in eukaryotic cytokinesis, *Curr. Biol.* **26**, R719 (2016).
 [4] Z. McDargh, S. Wang, H. F. Chin, S. Thiyagarajan, E. Karatekin, T. D. Pollard, and B. O’Shaughnessy, Myosins generate contractile force and maintain organization in the cytokinetic contractile ring, [10.1101/2021.05.02.442363](https://doi.org/10.1101/2021.05.02.442363).
 [5] L. T. Nguyen, M. T. Swulius, S. Aich, M. Mishra, and G. J. Jensen, Coarse-grained simulations of actomyosin rings point to a nodeless model involving both unipolar and bipolar myosins, *Mol. Biol. Cell* **29**, 1318 (2018).
 [6] S. Thiyagarajan, S. Wang, and B. O’Shaughnessy, A node organization in the actomyosin contractile ring generates tension and aids stability, *Mol. Biol. Cell* **28**, 3286 (2017).
 [7] M. Murrell, P. W. Oakes, M. Lenz, and M. L. Gardel, Forcing cells into shape: The mechanics of actomyosin contractility, *Nat. Rev. Mol. Cell Biol.* **16**, 486 (2015).
 [8] D. B. Oelz, B. Y. Rubinstein, and A. Mogilner, A combination of actin treadmilling and cross-linking drives contraction of random actomyosin arrays, *Biophys. J.* **109**, 1818 (2015).
 [9] H. Turlier, B. Audoly, J. Prost, and J.-F. Joanny, Furrow constriction in animal cell cytokinesis, *Biophys. J.* **106**, 114 (2014).
 [10] Y.-W. Jung and M. Mascagni, Constriction model of actomyosin ring for cytokinesis by fission yeast using a two-state sliding filament mechanism, *J. Chem. Phys.* **141**, 125101 (2014).
 [11] X. Ma, M. Kovács, M. A. Conti, A. Wang, Y. Zhang, J. R. Sellers, and R. S. Adelstein, Nonmuscle myosin II exerts tension but does not translocate actin in vertebrate cytokinesis, *Proc. Natl. Acad. Sci. U.S.A.* **109**, 4509 (2012).
 [12] I. Mendes Pinto, B. Rubinstein, and R. Li, Force to divide: Structural and mechanical requirements for actomyosin ring contraction, *Biophys. J.* **105**, 547 (2013).
 [13] I. Mendes Pinto, B. Rubinstein, A. Kucharavy, J. R. Unruh, and R. Li, Actin depolymerization drives actomyosin ring contraction during budding yeast cytokinesis, *Dev. Cell* **22**, 1247 (2012).
 [14] M. Lord, E. Laves, and T. D. Pollard, Cytokinesis depends on the motor domains of myosin-II in fission yeast but not in budding yeast, *Mol. Biol. Cell* **16**, 5346 (2005).
 [15] Z. Lansky, M. Braun, A. Lüdecke, M. Schlierf, P. R. ten Wolde, M. E. Janson, and S. Diez, Diffusible crosslinkers generate directed forces in microtubule networks, *Cell* **160**, 1159 (2015).
 [16] O. Kučera, V. Sahaan, D. Janda, S. H. Dijkstra, E. Pilátová, E. Zatecka, S. Diez, M. Braun, and Z. Lansky, Anillin propels myosin-independent constriction of actin rings, *Nat. Commun.* **12**, 4595 (2021).
 [17] H. Wierenga and P. R. ten Wolde, Diffusible Cross-Linkers Cause Superexponential Friction Forces, *Phys. Rev. Lett.* **125**, 078101 (2020).
 [18] H. Wierenga, Statistical mechanics of cytoskeletal filaments, Ph.D. thesis, Vrije Universiteit, Amsterdam, 2021.
 [19] See Supplemental Material at <http://link.aps.org/supplemental/10.1103/PhysRevLett.131.038401> for discussion of model parameters and configuration space assumptions, derivations of the ring bending energy and friction

- coefficients, and Supplemental figures, which includes Refs. [20–43].
- [20] S. Jananji, C. Risi, I. K. Lindamulage, L.-P. Picard, R. Van Sciver, G. Laflamme, A. Albaghjati, G. R. Hickson, B. H. Kwok, and V. E. Galkin, Multimodal and polymorphic interactions between anillin and actin: Their implications for cytokinesis, *J. Mol. Biol.* **429**, 715 (2017).
- [21] J. van Mameren, K. C. Vermeulen, F. Gittes, and C. F. Schmidt, Leveraging single protein polymers to measure flexural rigidity, *J. Phys. Chem. B* **113**, 3837 (2009).
- [22] Y. Arai, R. Yasuda, K.-i. Akashi, Y. Harada, H. Miyata, K. Kinoshita, and H. Itoh, Tying a molecular knot with optical tweezers, *Nature (London)* **399**, 446 (1999).
- [23] D. Arndt, W. Bangerth, D. Davydov, T. Heister, L. Heltai, M. Kronbichler, M. Maier, J.-P. Pelteret, B. Turcksin, and D. Wells, The DEAL.II finite element library: Design, features, and insights, *Comput. Math. Appl.* **81**, 407 (2021).
- [24] D. Arndt, W. Bangerth, B. Blais, M. Fehling, R. Gassmüller, T. Heister, L. Heltai, U. Köcher, M. Kronbichler, M. Maier, P. Munch, J.-P. Pelteret, S. Proell, K. Simon, B. Turcksin, D. Wells, and J. Zhang, The DEAL.II library, version 9.3, *J. Numer. Math.* **29**, 171 (2021).
- [25] H. Kojima, A. Ishijima, and T. Yanagida, Direct measurement of stiffness of single actin filaments with and without tropomyosin by *in vitro* nanomanipulation, *Proc. Natl. Acad. Sci. U.S.A.* **91**, 12962 (1994).
- [26] I. M. Sokolov, Ito, Stratonovich, Hänggi and all the rest: The thermodynamics of interpretation, *Chem. Phys.* **375**, 359 (2010).
- [27] M. Yang and M. Ripoll, Brownian motion in inhomogeneous suspensions, *Phys. Rev. E* **87**, 062110 (2013).
- [28] G. Li and J. X. Tang, Diffusion of actin filaments within a thin layer between two walls, *Phys. Rev. E* **69**, 061921 (2004).
- [29] S. Broersma, Viscous force and torque constants for a cylinder, *J. Chem. Phys.* **74**, 6989 (1981).
- [30] S. Broersma, Viscous force constant for a closed cylinder, *J. Chem. Phys.* **32**, 1632 (1960).
- [31] *CRC Handbook of Chemistry and Physics*, edited by W. M. Haynes, 97th edition (CRC Press, Taylor & Francis Group, Boca Raton, 2016).
- [32] C. P. Brangwynne, G. H. Koenderink, E. Barry, Z. Dogic, F. C. MacKintosh, and D. A. Weitz, Bending dynamics of fluctuating biopolymers probed by automated high-resolution filament tracking, *Biophys. J.* **93**, 346 (2007).
- [33] H. Isambert, P. Venier, A. C. Maggs, A. Fattoum, R. Kassab, D. Pantaloni, and M.-F. Carlier, Flexibility of actin filaments derived from thermal fluctuations: Effect of bound nucleotide, phalloidin, and muscle regulatory proteins, *J. Biol. Chem.* **270**, 11437 (1995).
- [34] A. Ott, M. Magnasco, A. Simon, and A. Libchaber, Measurement of the persistence length of polymerized actin using fluorescence microscopy, *Phys. Rev. E* **48**, R1642 (1993).
- [35] F. Gittes, B. Mickey, J. Nettleton, and J. Howard, Flexural rigidity of microtubules and actin filaments measured from thermal fluctuations in shape, *J. Cell Biol.* **120**, 923 (1993).
- [36] R. Dominguez and K. C. Holmes, Actin structure and function, *Annu. Rev. Biophys.* **40**, 169 (2011).
- [37] E. Evans and K. Ritchie, Dynamic strength of molecular adhesion bonds, *Biophys. J.* **72**, 1541 (1997).
- [38] G. I. Bell, Models for the specific adhesion of cells to cells, *Science* **200**, 618 (1978).
- [39] L. Jiang, Y. Gao, F. Mao, Z. Liu, and L. Lai, Potential of mean force for protein–protein interaction studies, *Proteins: Struct., Funct., Bioinf.* **46**, 190 (2002).
- [40] C. Rackauckas and Q. Nie, DifferentialEquations.jl—A performant and feature-rich ecosystem for solving differential equations in JULIA, *J. Open Res. Software* **5**, 15 (2017).
- [41] C. Rackauckas and Q. Nie, Adaptive methods for stochastic differential equations via natural embeddings and rejection sampling with memory, *Discrete Contin. Dyn. Sys.—B* **22**, 2731 (2017).
- [42] C. Rackauckas and Q. Nie, Stability-optimized high order methods and stiffness detection for pathwise stiff stochastic differential equations, [arXiv:1804.04344](https://arxiv.org/abs/1804.04344).
- [43] A. Cumberworth and P. R. ten Wolde, Data set for the replication package of the paper “Constriction of actin rings by passive crosslinkers”, [10.5281/zenodo.6327217](https://zenodo.org/record/6327217) (2022).
- [44] K. Matsuda, M. Sugawa, M. Yamagishi, N. Kodera, and J. Yajima, Visualizing dynamic actin cross-linking processes driven by the actin-binding protein anillin, *FEBS Lett.* **594**, 1237 (2020).
- [45] A. Jegou and G. Romet-Lemonne, The many implications of actin filament helicity, *Semin. Cell Dev. Biol.* **102**, 65 (2020).
- [46] V. Ropars, Z. Yang, T. Isabet, F. Blanc, K. Zhou, T. Lin, X. Liu, P. Hissier, F. Samazan, B. Amigues, E. D. Yang, H. Park, O. Pylypenko, M. Cecchini, C. V. Sindelar, H. L. Sweeney, and A. Houdusse, The myosin X motor is optimized for movement on actin bundles, *Nat. Commun.* **7**, 12456 (2016).
- [47] A. Vilfan, Twirling motion of actin filaments in gliding assays with nonprocessive myosin motors, *Biophys. J.* **97**, 1130 (2009).
- [48] J. F. Beausang, H. W. Schroeder, P. C. Nelson, and Y. E. Goldman, Twirling of actin by myosins II and V observed via polarized TIRF in a modified gliding assay, *Biophys. J.* **95**, 5820 (2008).
- [49] M. Y. Ali, S. Uemura, K. Adachi, H. Itoh, K. Kinoshita, and S. Ishiwata, Myosin V is a left-handed spiral motor on the right-handed actin helix, *Nat. Struct. Biol.* **9**, 464 (2002).
- [50] I. Sase, H. Miyata, S. Ishiwata, and K. Kinoshita, Axial rotation of sliding actin filaments revealed by single-fluorophore imaging, *Proc. Natl. Acad. Sci. U.S.A.* **94**, 5646 (1997).
- [51] S. P. S. Deopa, S. S. Rajput, A. Kumar, and S. Patil, Direct and simultaneous measurement of the stiffness and internal friction of a single folded protein, *J. Phys. Chem. Lett.* **13**, 9473 (2022).
- [52] H. Nakagawa and M. Kataoka, Rigidity of protein structure revealed by incoherent neutron scattering, *Biochim. Biophys. Acta, Gen. Subj.* **1864**, 129536 (2020).
- [53] M. Grimaldo, F. Roosen-Runge, F. Zhang, F. Schreiber, and T. Seydel, Dynamics of proteins in solution, *Q. Rev. Biophys.* **52**, e7 (2019).

- [54] H. Ahmadzadeh, D. H. Smith, and V. B. Shenoy, Viscoelasticity of tau proteins leads to strain rate-dependent breaking of microtubules during axonal stretch injury: Predictions from a mathematical model, *Biophys. J.* **106**, 1123 (2014).
- [55] C.-Y. Tseng, A. Wang, G. Zocchi, B. Rolih, and A. J. Levine, Elastic energy of protein-DNA chimeras, *Phys. Rev. E* **80**, 061912 (2009).
- [56] M. Dong, S. Husale, and O. Sahin, Determination of protein structural flexibility by microsecond force spectroscopy, *Nat. Nanotechnol.* **4**, 514 (2009).
- [57] I. Aprodu, M. Soncini, and A. Redaelli, Mechanical characterization of motor proteins: A molecular dynamics approach, *Macromol. Theory Simul.* **17**, 376 (2008).
- [58] M. Kawakami, K. Byrne, D. J. Brockwell, S. E. Radford, and D. A. Smith, Viscoelastic study of the mechanical unfolding of a protein by AFM, *Biophys. J.* **91**, L16 (2006).
- [59] S. Jeney, E. H. K. Stelzer, H. Grubmüller, and E.-L. Florin, Mechanical properties of single motor molecules studied by three-dimensional thermal force probing in optical tweezers, *Chem. Phys. Chem.* **5**, 1150 (2004).
- [60] G. Zaccai, How soft is a protein? A protein dynamics force constant measured by neutron scattering, *Science* **288**, 1604 (2000).
- [61] T. A. J. Duke, Molecular model of muscle contraction, *Proc. Natl. Acad. Sci. U.S.A.* **96**, 2770 (1999).
- [62] M. R. Stachowiak, C. Laplante, H. F. Chin, B. Guirao, E. Karatekin, T. D. Pollard, and B. O’Shaughnessy, Mechanism of cytokinetic contractile ring constriction in fission yeast, *Dev. Cell* **29**, 547 (2014).
- [63] M. Malla, T. D. Pollard, and Q. Chen, Counting actin in contractile rings reveals novel contributions of cofilin and type II myosins to fission yeast cytokinesis, *Mol. Biol. Cell* **33**, ar51 (2022).
- [64] M. T. Swulius, L. T. Nguyen, M. S. Ladinsky, D. R. Ortega, S. Aich, M. Mishra, and G. J. Jensen, Structure of the fission yeast actomyosin ring during constriction, *Proc. Natl. Acad. Sci. U.S.A.* **115**, E1455 (2018).
- [65] N. Courtemanche, T. D. Pollard, and Q. Chen, Avoiding artefacts when counting polymerized actin in live cells with LifeAct fused to fluorescent proteins, *Nat. Cell Biol.* **18**, 676 (2016).
- [66] Z. Zhou, E. L. Munteanu, J. He, T. Ursell, M. Bathe, K. C. Huang, and F. Chang, The contractile ring coordinates curvature-dependent septum assembly during fission yeast cytokinesis, *Mol. Biol. Cell* **26**, 78 (2015).
- [67] S. Thiagarajan, E. L. Munteanu, R. Arasada, T. D. Pollard, and B. O’Shaughnessy, The fission yeast cytokinetic contractile ring regulates septum shape and closure, *J. Cell Sci.* **128**, 3672 (2015).
- [68] F. Chang, Forces that shape fission yeast cells, *Mol. Biol. Cell* **28**, 1819 (2017).
- [69] P. A. Fantes and C. S. Hoffman, A brief history of *Schizosaccharomyces pombe* research: A perspective over the past 70 years, *Genetics* **203**, 621 (2016).
- [70] Y. P. Bhavsar-Jog and E. Bi, Mechanics and regulation of cytokinesis in budding yeast, *Semin. Cell Dev. Biol.* **66**, 107 (2017).
- [71] S. Chen, T. Markovich, and F. C. MacKintosh, Motor-Free Contractility in Active Gels, *Phys. Rev. Lett.* **125**, 208101 (2020).
- [72] M. Miyazaki, M. Chiba, H. Eguchi, T. Ohki, and S. Ishiwata, Cell-sized spherical confinement induces the spontaneous formation of contractile actomyosin rings *in vitro*, *Nat. Cell Biol.* **17**, 480 (2015).
- [73] L. Sun, R. Guan, I.-J. Lee, Y. Liu, M. Chen, J. Wang, J.-Q. Wu, and Z. Chen, Mechanistic insights into the anchorage of the contractile ring by anillin and Mid1, *Dev. Cell* **33**, 413 (2015).
- [74] J. Schöneberg, M. R. Pavlin, S. Yan, M. Righini, I.-H. Lee, L.-A. Carlson, A. H. Bahrami, D. H. Goldman, X. Ren, G. Hummer, C. Bustamante, and J. H. Hurley, ATP-dependent force generation and membrane scission by ESCRT-III and Vps4, *Science* **362**, 1423 (2018).
- [75] E. Beltrán-Heredia, V. G. Almendro-Vedia, F. Monroy, and F. J. Cao, Modeling the mechanics of cell division: Influence of spontaneous membrane curvature, surface tension, and osmotic pressure, *Frontiers of oral physiology* **8**, 312 (2017).
- [76] L. Olivi, M. Berger, R. N. P. Creighton, N. De Franceschi, C. Dekker, B. M. Mulder, N. J. Claassens, P. R. ten Wolde, and J. van der Oost, Towards a synthetic cell cycle, *Nat. Commun.* **12**, 4531 (2021).